Surface effects on exciton diffusion in non polar ZnO/ZnMgO heterostructures

Georges Sakr, Corinne Sartel, Vincent Sallet, Alain Lusson, Gilles Patriarche, Pierre Galtier, Julien Barjon

Surface effects on exciton diffusion in non polar ZnO/ZnMgO heterostructures

G Sakr[1], C Sartel[1], V Sallet[1], A Lusson[1], G Patriarche[2], P Galtier[1] and J Barjon[1]

[1]GEMaC, Université de Versailles St Quentin en Yvelines, CNRS, Université Paris-Saclay, 45 avenue des Etats-Unis, 78035 Versailles Cedex, France
[2]LPN CNRS, UPR20, 91460 Marcoussis, France

The diffusion of excitons injected in ZnO/$Zn_{0.92}Mg_{0.08}O$ quantum well heterostructures grown by metal-organic-vapor-phase-epitaxy on non-polar ZnO substrates is investigated at room temperature. Cathodoluminescence linescans in a field-emission-gun scanning-electron-microscope are performed across cleaved cross-sections. A 55 nm diffusion length is assessed for excitons in bulk ZnMgO. When prepared as small angle bevels using focused ion beam (FIB), the effective diffusion length of excitons is shown to decrease down to 8 nm in the thinner part of the slab. This effect is attributed to non-radiative surface recombinations, with a 7×10^4 cm s^{-1} recombination velocity estimated at the FIB-machined ZnMgO surface. The strong reduction of the diffusion extent in such thin lamellae usually used for transmission electron microscopy could be use improve the spatial resolution of cathodoluminescence images, often limited by diffusion processes.

Keywords: excitons, diffusion, heterostructures, cathodoluminescence

1. Introduction

Diffusion lengths of excess charge carriers are key parameters which monitor semiconductor devices under injection. They directly impact the performances of optoelectronic devices—dedicated to light emission (LEDs, lasers) or absorption (photodetectors, solar panels). The diffusion properties of the injected excess charge carriers obviously relies on (i) the operating temperature (ii) the intrinsic properties of the material (iii) the density and nature of the defects it contains depending on the growth method used, but also (iv) on surface effects which may become dominant when nanosized objects are involved. From a characterization point of view, the diffusion properties of excess carriers are also a strong limitation for the spatial resolution of cathodoluminescence images: the spatial extent of charge carriers caused by diffusion is most often much larger than the probe beam size. More generally, it is clear that there is a need for nondestructive characterization tools able to measure diffusion lengths on real objects with a suitable accuracy.

The diffusion length is given by $L = \sqrt{D\tau}$, where D is the diffusivity and τ the lifetime of carriers injected in excess. The range of carrier diffusion lengths in bulk semiconductors is extremely wide: it covers the *millimeter* to the *nanometer* scale, depending on the crystal quality and purity. In indirect semiconductors, large carrier lifetimes are generally responsible for long-range diffusion (e.g. up to 1.2 mm in pure silicon (Saritas and McKell 1988), a few 10 μm in pure diamond (Barjon *et al* 2012). At comparable doping, the spatial extent of diffusion is generally much shorter in direct semiconductors due to faster recombination of excess charge carriers. In the presence of impurities and defects, carrier diffusion lenghts fall in the nanometer range (Gustafsson *et al* 1998, Barjon *et al* 2003).

For diffusion lengths which reach values noticeably below the micrometer range, it becomes necessary to use techniques

with a precise excitation control at the nanometer scale. In the recent years, cathodoluminescence (CL) setups have been fitted to SEM equipped with field emission gun (FEG). They are capable to supply nanometer sized probes at low voltages for the investigation of semiconductor nanostructures (Matsuo *et al* 1996, Sekiguchi *et al* 2004, Phillips 2006). This kind of set-ups opens the way to perform direct diffusion measurements by optical and contactless technique with an accuracy of few nanometers.

Since several years, ZnO has been the subject of intense researches because of its wide band gap energy (3.3 eV) which makes this material interesting for optoelectronic devices emitting in the visible and near UV range (Klingshirn *et al* 2010). For this purpose, material studies have been undertaken to develop band-gap engineering expertise involving essentially ZnO/ZnMgO or ZnO/ZnCdO systems to fabricate well defined 2D or 1D heterostructures or quantum wells. In this context, the understanding and optimization of the excess charge properties of ZnO and related alloys are an important issue for the realization of efficient optoelectronic devices.

Even without intentional doping, ZnO and ZnMgO crystals generally present a n-type electrical conductivity with high concentrations of free electrons/cm^3 at room temperature. Such a doping favors the exciton population with respect to the free carrier one. In the case of ZnO with an exciton binding energy of 60 meV and $n = 10^{18}$ cm^{-3}, the mass action law (Im *et al* 1997) indicates that the exciton density is about one hundred times superior to the free charge carriers at 300 K in weak excitation regime. That is the reason why, in the following recombination and diffusion processes are considered as governed by excitons.

Few studies have been reported on exciton diffusion lengths in bulk ZnO and ZnMgO (Zippel *et al* 2009, Noltemeyer *et al* 2012). Values ranging from 75 nm to 220 nm were measured depending on the temperature and the content on Mg. For bulk ZnO, the behavior of exciton diffusion with increasing temperature has been interpreted by scattering processes involving deformation and Fröhlich potentials. Lower values are observed for ZnMgO alloys. On the other hand, exciton diffusion in ZnO-based nanowires has attracted more attention (Yoo and Dang 2008, Hwang *et al* 2011, Donatini *et al* 2016a). Beside this, the problematic influence of non-radiative surface recombination was pointed out some time ago (Bylander 1978, Zhao *et al* 2008). This obviously must be taken into account to correctly interpret experimental diffusion length measurement particularly for the design and optimization of nanostructures-based optoelectronic devices.

In this paper, cathodoluminescence is used to measure the diffusion length of excitons in bulk ZnMgO at room temperature thanks to specifically designed samples. The effects of non-radiative surface recombination are evidenced with small angle beveled samples prepared using focused ion beam (FIB). It is responsible for a strong shrinking of the diffusion range in nanometer-thick FIB lamella. This kind of thin-lamella preparation, usually dedicated to transmission electron microscopy, have a strong potential to improve the spatial resolution of CL images.

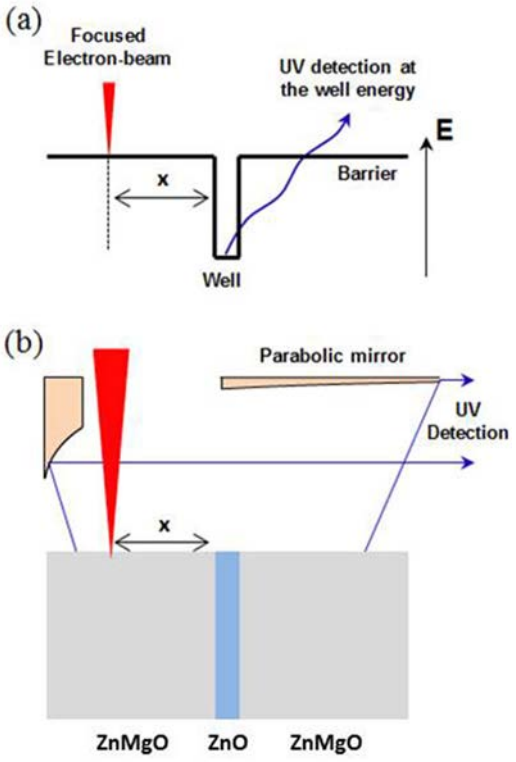

Figure 1. (a) Basic principle of a 1D diffusion experiment. (b) CL experimental configuration (3D): the electron beam is scanned perpendicularly to a single QW ZnO/ZnMgO sample prepared as a cross section.

2. Method, samples and experimental conditions

2.1. CL diffusion experiment

The basic principle of CL diffusion experiments presented in this work is illustrated at one dimension (1D) in figure 1(a). Like in a pump-probe experiment, excitons are locally generated under an electron beam focused on the barrier at a distance x (pump) from a collecting well (probe). Excitons diffusing in the barrier are collected in the well where they recombine radiatively. Re-absorption of the light emitted by the well does not occur in the barrier which has larger bandgap energy.

In steady-state regime, the exact solution of the 1D diffusion equation is particularly simple. The density of excitons $n(x)$ collected in the well as a function of the distance x to the well writes $n(x) = n(0)\exp(-x/L)$, where L is the diffusion length of excitons *in the barrier* material. Assuming that the intensity of radiative recombinations in the well is proportional to its population $n(x)$, the study of $I(x)$ as a function of the distance x to the well provides a measurement of the diffusion length of excitons *in the barrier*, by using:

$$I(x) = I(0)\exp(-x/L). \quad (1)$$

In practice, the CL diffusion experiments are three dimensional (3D). The experimental configuration used here to measure exciton diffusion by cathodoluminescence is shown in figure 1(b). CL linescan acquisitions are performed on a cross section of the specimen in order to record $I(x)$ along a line perpendicular to the well plane. As soon as the non-radiative

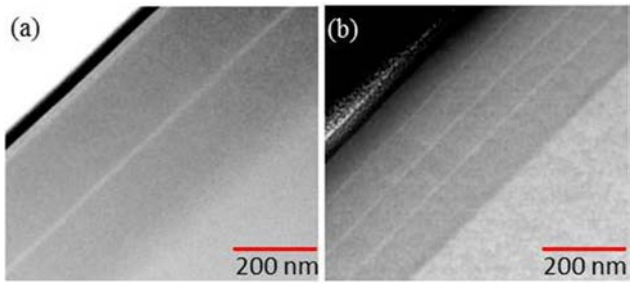

Figure 2. HAADF STEM images: (a) sample *A* with a single ZnO QW embedded in $Zn_{0.92}Mg_{0.08}O$ barriers; (b) sample *B* with three ZnO QWs. ZnO QWs appear bright and ZnMgO layers appear darker. The heterostructures were grown on (1 1 − 2 0) non-polar ZnO substrates.

surface recombination velocity v_s is negligible, the solution of the 3D diffusion equation in this geometry is the same than (equation (1)) at 1D (Berz and Kuiken 1976). Such an experiment might be used to assess the 3D diffusion length L_{3D} occurring in the bulk of the crystal. However, care has to be taken to check the validity of the $v_s \approx 0$ assumption, as seen later.

The geometry of thin lamellas, such as studied in Part 4 with FIB preparation, is almost bidimensionnal (2D). In the case of a collecting line, equation (1) is also valid without any assumption. However the extracted diffusion lengths L_{2D} will have a different physical meaning, as discussed in Part (4).

2.2. Samples and their preparation

Two samples (referenced *A* and *B*) were homo-epitaxially grown by metal organic vapor phase epitaxy (MOVPE) on ZnO substrates (supplied by CrysTec GmbH) orientated on the *A*-plane (1 1 − 2 0). Sample *A* consists of a single ZnO quantum well (QW) embedded in $Zn_{0.92}Mg_{0.08}O$ barriers, while three ZnO QWs are embedded in sample *B*. The *A*-plane is non polar, which avoids the appearance of electrical fields along the growth direction causing a quantum confined Stark effect. The choice of non-polar crystals is important for the correct realization of diffusion experiments: the absence of polarization ensures a constant radiative efficiency of the QW upon the collected carrier density.

For the MOVPE process, diethyl-zinc (DEZn), bis-methylcyclopentadienyl-magnesium ($(MCp)_2Mg$), and nitrous oxide (N_2O) have been used as zinc, magnesium, and oxygen sources, respectively. Carrier gas was helium. The ZnO quantum wells and ZnMgO barriers were deposited at 950 °C under high VI/II mole ratio ($R_{VI/II} > 6000$) to obtain a bi-dimensional growth and smooth surfaces. Reactor pressure was 50 Torr.

Figure 2 shows scanning transmission electron microscopy (STEM) images performed using a Jeol 2200FS microscope. They were acquired using a high angular annular dark field (HAADF) detector, giving a contrast which is proportional to the material density. As a result, ZnO appears bright while the lighter ZnMgO alloy appears dark. The images show that barriers in sample *A* are 176 nm thick. In sample *B*, the three QWs are embedded between 70/83/80/110 nm thick barriers. The energy of the excitonic emission from the QW is observed at 3.34 eV (Chauveau *et al* 2008) at 300 K which is coherent with a 3 nm QW thickness. This value is also close to the 5 nm nominal thickness of the QW estimated from the growth rate. The narrow linewidth (7 meV) of the QW CL recorded at low temperature (see supplementary information figure S1 (stacks.iop.org/JPhysCM/29/485706/mmedia)) indicates the good quality of the wells. The magnesium composition of the alloyed barriers is measured by energy-dispersive x-ray spectroscopy (EDX) at 8%. Hall effect measurements on a $Zn_{0.92}Mg_{0.08}O$ layer grown in similar conditions on a sapphire substrate shows that majority carriers are free electrons with $n = 3.4 \times 10^{17}$ cm^{-3} at 300 K. No extended defects such as threading dislocations are observed by STEM, due to a weak lattice mismatch between ZnO and $Zn_{0.92}Mg_{0.08}O$ epilayers (Kaschner *et al* 2002) ensuring negligible strain effects. The total thicknesses of the homoepitaxial stackings is 355 nm, almost identical for samples *A* and *B*.

For diffusion experiments, the samples were prepared as cross sections by two different techniques. The first one is a cleavage along the *c*-plane. This preparation will be used (part 3) to measure the diffusion length of excess charge carriers in the bulk ZnMgO barrier. The second is the preparation of thin cross sections by the focused ion beam (FIB) technique. It was performed with 30 keV Ga ions. For the finishing step, the ion voltage was reduced to 5–7 keV to minimize the surface amorphization. With this procedure, thin slabs of sample *A* and *B* were prepared in a bevel geometry, with an angle of about 2 degrees. As a result, the sample thickness, labeled t, regularly decreases from 300 nm to 0 nm, as checked with scanning electron microscope (SEM) images. CL linescans were realized for different thicknesses of thin FIB samples. Thanks to contamination marks clearly visible in SEM, it was possible to measure the blade thickness exactly where each linescan CL was performed. Such experiments will be dedicated (Part 4) to probe the effects of surface recombination on exciton diffusion.

2.3. CL experiments: accurate control of the excitation location with a FEG-SEM

Samples are excited locally with the focused electron beam of an SEM *JEOL 7001F* equipped with a field effect gun (FEG). The collection of the radiative exciton recombinations in the QW is realized thanks to a *RPM2000* parabolic mirror and analyzed with a *Horiba Jobin Yvon* optical system equipped with the *CL Link* e-beam drive unit (developed in collaboration with GEMaC). The excitonic luminescence from the well is spectrally selected using a *TRIAX550* monochromator equipped with a silicon CCD camera. CL images are also recorded using a UV photomultiplier *Hamamatsu* mounted on the second exit port of the monochromator. All the diffusion experiments are performed at 300 K.

The lateral extension r_g of the electron–hole pair generation volume is the relevant parameter to estimate the accuracy of the diffusion-length measurement:

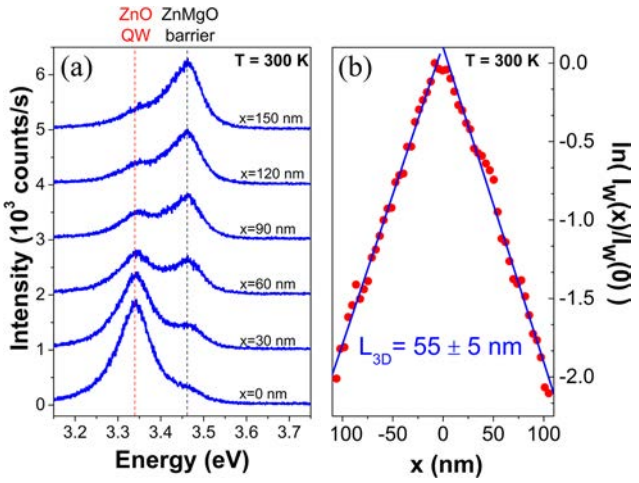

Figure 3. (a) Room-temperature CL spectra collected from the cleaved cross-section when exciting at different distances x from the QW. The spectra are shifted vertically for a better clarity. (b) A linear regression on the logarithmic of $I_W(x)/I_W(0)$ is used to measure L, the diffusion length of excitons in ZnMgO (details in the text). The step between two electron beam impacts is ~4 nm. The incident electron energy is $E_0 = 2.5$ keV and the electron beam current $i = 0.1$ nA.

$$r_g = \sqrt{\varnothing^2 + \sigma^2} \qquad (2)$$

where $\varnothing$ is the electron beam diameter focused at the specimen surface and σ is the lateral spread due to the electron scattering within matter (see supplementary materials figure S2). When using a FEG gun, the electron beam diameter is a few nanometer size. For instance in the conditions used here: $\varnothing \approx 3$ nm at 2.5 keV and $\varnothing \approx 1.5$ nm at 30 keV according to SEM manufacturer specifications.

The best accuracy in CL diffusion experiments are achieved according to different strategies in the cases (i) of the semi-infinite 3D medium formed by a cleaved cross-section or (ii) of the quasi-2D systems formed by FIB thin slabs. Table 1 shows the calculated values of σ by using Monte-Carlo simulations (Casino software (Drouin *et al* 2007)) of electrons accelerated on a bulk ZnO crystal or on thin slabs of 100 and 20 nm thicknesses (supplementary materials figure S2). In the bulk case (i), σ increases with E_0, so that *low acceleration-voltages* are preferred. In case (ii), at *high acceleration-voltages* the thin lamellae become transparent which strongly reduces σ. On the basis of table 1 and equation (2), we found $r_g = 8.2$ nm at 2.5 keV in bulk ZnO, $r_g = 2.6$ nm in a 100 nm-thick preparation at 30 keV and $r_g = 1.5$ nm in a 20 nm-thick preparation at 30 keV. These values indicate the spatial resolution of the diffusion length measurements with a FEG-SEM, hereafter.

3. Bulk diffusion length of excitons in ZnMgO ternary alloy

3.1. Experiment on the cleaved cross-section (sample A)

In figure 3(a) CL spectra from the cleaved cross section of sample *A* are reported for different distances x from the QW. For an excitation located far from the QW, the barrier luminescence predominates in the spectra with a maximum at 3.46 eV. The CL intensity emitted from the ZnO QW appears only very weak at 3.34 eV. When the distance x between the generation region and the QW decreases, the light emission intensities simultaneously increase for the QW and decrease for the ZnMgO barrier. These observations highlight the efficient transfer of excitons from the ZnMgO barrier to the ZnO QW. At $x = 0$, the QW CL intensity reaches a maximum, since the incident electron beam directly impacts the QW.

Table 1. Lateral spread σ of the electron beam in ZnO calculated by Monte-Carlo simulations (see conditions in the supplementary information figure S2).

ZnO sample	σ (2.5 keV)	σ (30 keV)
Bulk	7.7 nm	550 nm
100 nm thick	7.7 nm	1.9 nm
20 nm thick	0.9 nm	<0.1 nm

In figure 3(b) $\ln(I_W(x)/I_w(0))$ is plotted as a function of x. The data plot is clearly linear and is well symmetrical in the upper and lower ZnMgO layers. According to equation (2), a linear regression on such a plot gives the diffusion length of excitons in the barrier. We found $L = 55 \pm 5$ nm in the ZnMgO barrier at room temperature along a-direction. Note that in principle this diffusion length should be considered as an effective diffusion length since it takes into account the recombination velocity at the cleaved surface. However, the observation of a linear behavior over 2 decades indicates that the effective diffusion length of 55 nm is very close to the bulk value (Donolato 1982). This will be further confirmed in Part 4.

The result of the diffusion experiment is consistent with the order of magnitude of 75 nm reported by Zippel *et al* (2009) for $ZnO/Zn_{0.83}Mg_{0.17}O$ heterostructures grown by pulsed laser deposition. The diffusion length in the ZnMgO ternary alloy is found lower than the 110 nm value reported in bulk ZnO (Noltemeyer *et al* 2012). This is consistent with a general trend to observe a lower extent of the carrier diffusion in a ternary than in binary semiconductor compounds (Gustafson 1998). First, the growth conditions of ternary alloys are more difficult to control so that they generally present a higher density of defects compared to binary compounds. Second, the scattering of carriers on the potential fluctuations—statistical or due to composition inhomogeneities—probably also contributes to limit the extent of exciton diffusion in ternary alloys.

3.2. Luminescence efficiency of QW heterostructures

To check the consistency of previous diffusion results, CL experiments were also performed as a function of the incident electron beam energy in the more conventional configuration shown in inset of figure 4: Incident electrons are oriented along the growth axis and impact the as-grown surface. The beam current i was adjusted in order to keep a constant 0.6 μW excitation power ($P = iE_0$). Figure 4 then provides a comparison of sample *A* and *B* luminescence yields, with either 1 or 3 QWs. The CL of a bulk ZnO single crystal (CrysTec substrate) recorded in the same conditions is also shown for comparison.

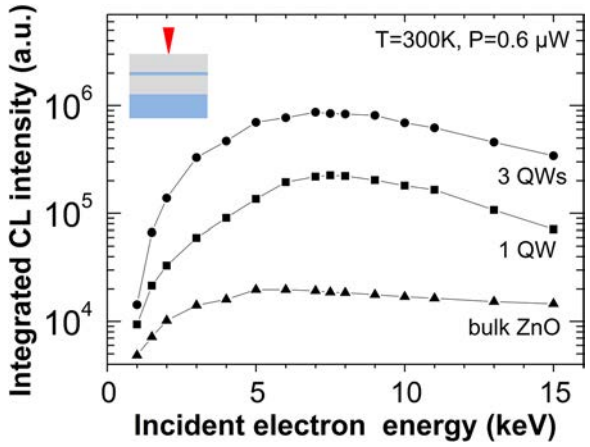

Figure 4. Integrated CL intensity emitted as a function of the incident electron energy E_0. The excitation geometry is shown in inset and a bulk ZnO sample is presented for comparison. The incident power $P = iE_0$ was kept to a constant value of 0.6 μW.

In all samples, the CL intensity drops at low voltage. This is an effect of non-radiative recombinations occurring at the sample surface. Indeed, the lower the incident electron energy, the closer the carriers are injected from the surface and the higher the luminescence losses by non-radiative surface recombinations. The maximum CL yield is observed for electrons of about 7–8 keV incident energy in ZnO QW samples. At higher energies, the CL emission decreases again because excitons are generated deeper, directly in the ZnO substrate rather than in the ZnMgO/ZnO/ZnMgO epitaxial layers. In the bulk ZnO substrate, excitons recombine with a much lower radiative efficiency than in a QW. The maxima of light emissions occur at 7–8 keV for both the single- and the three-QW heterostructures simply because the QWs are centered in the multilayers which have comparable thicknesses.

More interestingly, the CL yield is almost 4 times higher with 3 QWs than with a single QW. To interpret this result with respect to diffusion experiments presented previously, one has to consider that most of excitons are generated in the ZnMgO barrier rather than in the QW. Indeed, the direct excitation of QWs by energy losses of incident electrons is extremely weak. As a quantitative illustration, the QW is excited by only 3% of the deposited energy in sample *A* at 8 keV. In fact, the CL yield experiments of figure 4 reveal the ability of ZnO QWs to collect excitons diffusing in the ZnMgO layers. In sample *A* having a single QW, the diffusion length in ZnMgO ($L_{3D} = 55$ nm measured previously) is much shorter than the ZnMgO barrier thickness (175 nm), hence a large amount of excitons are lost. On the contrary in sample *B*, the diffusion length is comparable to the thicknesses of ZnMgO layers (70/83/80/110 nm). The 4 times higher luminescence yield of sample *B* is explained by a more efficient capture of excitons in the three QWs. As a summary, the CL yield of the samples is consistent with the 55 nm diffusion length found for bulk ZnMgO.

4. Surface recombinations in thin slabs prepared by FIB

In this part, the exciton diffusion is investigated in the quasi-2D geometry of thin beveled slabs prepared by FIB, as illustrated in figure 5(b). Linescans were performed across the single QW of sample *A* for different slab thicknesses *t*. Figure 5(a) shows the corresponding logarithmic plots. Again the $\ln(I_w(x)/I_w(0))$ plots present an almost linear form and effective diffusion lengths are deduced.

Figure 5(c) displays the dependency of the effective diffusion length in ZnMgO with the thicknesses t of the FIB preparation. The effective diffusion length in the thicker part ($t \sim 260$ nm) of the FIB bevel is 44 ± 12 nm. This result is consistent with the 55 nm diffusion length measured before from the cleaved cross section. A dramatic shrinkage of the diffusion extent is observed in the thinnest parts. In the thinnest regions of the FIB bevel ($t \sim 30$ nm), the effective diffusion length decreases down to 8 ± 2 nm. With high surface to volume ratios (*S*/*V*) in the thinnest part of the nanometric bevel, the influence of non-radiative surface recombinations is qualitatively expected to play a much more important role.

Quantitatively, the bulk diffusion length L_{3D} of injected carriers in ZnMgO has been assessed in Part 3 as $L_{3D} = \sqrt{D\tau_{3D}}$. In the 2D geometry of FIB lamellas investigated here, the effective diffusion lengths write $L_{2D} = \sqrt{D\tau_{2D}}$, where

$$\frac{1}{\tau_{2D}} = \frac{1}{\tau_{3D}} + \frac{1}{\tau_s}. \tag{3}$$

In this expression τ_{3D} is the lifetime of excitons in a bulk ZnMgO crystal and τ_s is the exciton lifetime at surface. For thin layers, the latter expresses with the surface recombination velocity (Langer and Walukiewicz 1995) v_s as $1/\tau_s = 2\, v_s/t$. The following expression is used as a first approach for describing the experimental results:

$$L_{2D} = L_{3D}\left(1 + \frac{2\,\tau_{3D}\,v_s}{t}\right)^{-1/2}. \tag{4}$$

For thin preparations, it indicates that the effective diffusion length is almost proportional to the square root of the preparation thickness. Given a bulk exciton lifetime in $Zn_{0.92}Mg_{0.08}O$ layers $\tau_{3D} = 0.4$ ns as measured by time-resolved cathodoluminescence (Donatini *et al* 2016b), v_s remains the only unknown parameter in equation (4). Our experimental results are reasonably well described by equation (4) with $v_s = 7 \times 10^4$ cm s^{-1} at the surface of ZnMgO (dashed line in figure 5(c)). Though the model deserves to be refined, this value is coherent with previous reports for v_s in ZnO found in the 1.5–4.5 $\times$ 10^5 cm s^{-1} range (Bylander 1978, Zhao *et al* 2008, Donatini *et al* 2016a). Surface defects induced by the ion bombardment during the FIB preparation might explain the higher recombination velocity observed here.

Finally, we found a reduced surface velocity $S = v_s\tau_{3D}/L_{3D}$ equal to about 5. This low *S* value means that the deviation

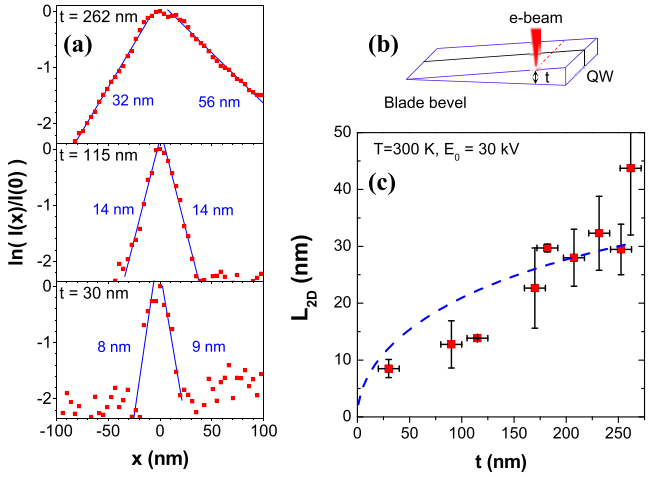

Figure 5. (a) CL linescans taken at different thicknesses, t, of the thin lamella prepared by FIB (sample A), substrate on the right. (b) Scheme of the corresponding experiment. (c) Effective diffusion length L_{2D} of excitons in ZnMgO as a function of the lamella thickness, t. Experiments done à 300 K with $E_0 = 30$ keV and $i = 0.1$ nA. The diffusion length values are averaged from both sides of the QW. The dashed curve is a plot of equation (4) with $v_s = 7 \times 10^4$ cm s^{-1} (details in the text).

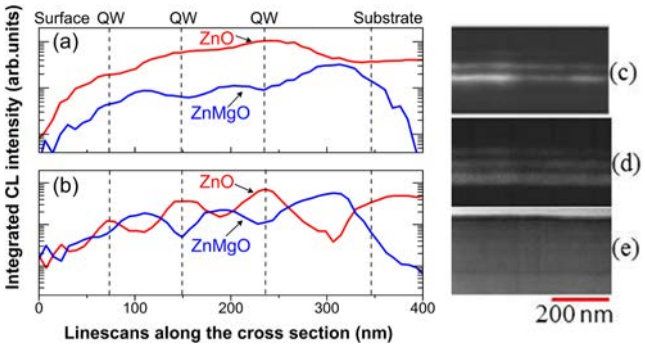

Figure 6. CL linescans along the cross section of sample B prepared by FIB: (a) thick region $t = 200$ nm, (b) thin region $t = 20$ nm. CL images obtained in the thin region when filtered at the luminescence energy of: (c) the ZnO QW and (d) the ZnMgO barrier (e) is a secondary electron image simultaneously recorded with the CL images.

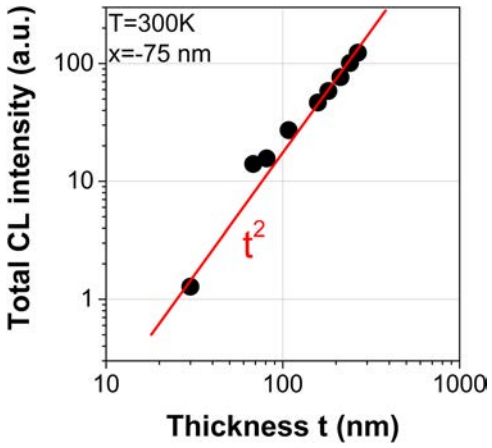

Figure 7. Total CL intensity as a function of the FIB preparation thickness recorded at $x = -75$ nm from the QW. The linear fit (red line) indicates that the CL intensity $I_{CL} \propto t^2$, where t is the thickness of the FIB cross-section.

from equation (2) due to surface recombinations is weak for the cleaved cross section investigated in Part 3. This confirms that the measurement $L_{3D} = 55$ nm is valid for excitons diffusing in the bulk of a ZnMgO crystal. An uncertainty below 30% can be further deduced from (Donolato 1982).

5. Application to high resolution CL images

There is a practical interest in using thin cross-section preparations for CL imaging. Actually, the spatial resolution of CL images is most often limited by the diffusion of excess charge carriers (or excitons in the present case). Indeed, the CL images are the combined result of excitation, diffusion and recombination processes. The luminescence signal obtained with a point-source excitation accounts for the spatial distribution of excess carriers by diffusion around the point-source. In other words, CL images might be seen as 'excitation images' meaning that they reveal the spatial distribution of injected excess carriers.

An expression $\sqrt{r_g{}^2 + 4L^2}$, where L is their effective diffusion length, was proposed in early times (Davidson 1977) for the CL image resolution. It has to be noted that it is not appropriate as a general description of the complex 3D diffusion and recombination problem leading to the formation of CL images (Donolato 1994). However, in the case of CL linescans and images of figure 6, the spatial resolution is limited by the diffusion length of excess carriers, as discussed in what follows.

CL linescans were performed on the slab bevel prepared from sample B with 3 QWs. Figure 6 compares the results obtained from the thick (~200 nm) and the thin (~20 nm) regions of the FIB preparation. For the thicker part (figure 6(a)) there is almost no variation of the luminescence intensity from the ZnO QWs. In other words, the QW emissions cannot be spatially separated because the distance between QWs is comparable to the carrier diffusion length in the ZnMgO barrier. On the contrary, in the thinner part (figure 6(b)) where the diffusion length is strongly reduced by surface recombinations, the ZnO signal exhibits strong spatial variations, which are fully correlated with opposite ones from the ZnMgO signal. Consequently, the identification of each QW becomes possible. This result is further illustrated in figures 6(c) and (d) where CL images from the thinnest part of the FIB lamella are strongly contrasted. The ZnO QW emissions are well spatially separated. These experiments highlight that, with thin FIB cross sections, the decrease of exciton diffusion due to surface effects significantly improves the spatial resolution of CL images.

However, the improvement of the spatial resolution in CL images has a cost. The counterpart of the diffusion length reduction is a strong CL signal decrease, which is evidenced in figure 7 as a function of the slab thickness. At $E_0 = 30$ keV, most of electrons are transmitted through the thin lamella (transparency regime). Then the energy absorbed

by the lamella is almost proportional to its thickness. In other words, the electron–hole generation rate g is proportional to t. As $\tau_{2D} \approx 2\ v_s/t$ in the thin lamella limit, the CL intensity $I = g\ (\tau_{2D}/\tau_{rad})$ is almost proportional to t^2 (Yuan *et al* 1989). In figure 7 we observe a good agreement with this simple description, showing that the effective diffusion length reduction is accompanied by a quadratic decrease of the luminescence efficiency. At the end, the improvement for the CL resolution with thin preparations appears as a matter of compromise between signal and resolution.

6. Conclusions

In this work, the diffusion of excitons injected in ZnMgO is investigated at the room temperature thanks to ZnO/ZnMgO non polar heterostructures. First, a diffusion length of 55 nm for excitons in ZnMgO is measured by CL linescans on a cleaved cross section. This value corresponds to the bulk diffusion length in the ZnMgO ternary alloy. It well explains the improved collection of excitons observed in multi-QW, attested by their higher luminescence yield compared with single QW structures. In the future, heterostructures based on ZnCdO/ZnO quantum wells appear promising to extend the proposed approach for the investigation of exciton diffusion in ZnO.

The effects of dimension reduction (3D $\rightarrow$ 2D) on exciton diffusion have been further studied with thin slabs prepared by FIB from the same samples. It is observed that the effective diffusion length is significantly reduced by non-radiative surface recombinations. Incidentally, thin preparations can be exploited to improve the spatial resolution of CL images in a compromise with the luminescence intensity reduction. A first order approach has been proposed to evaluate the recombination velocity, giving coherent values with published data. The model could be refined by a theoretical description of diffusion processes in the case of high incident electron energies, where a uniform generation line crosses electron-transparent samples, which has not been reported up to now.

Acknowledgments

The authors would like to thank D Troadec from IEMN, Villeneuve d'Ascq, France for the FIB bevel preparations and their thickness measurements. The authors are grateful to C Vilar for her precious technical help on the SEM-CL set-up, to E Chikoidze for Hall effect measurements and to M Phillips for stimulating discussions and to J Chevallier for his critical reading of the manuscript.

References

Barjon J, Jomard F, Tallaire A, Achard J and Silva F 2012 *Appl. Phys. Lett.* **100** 122107
Barjon J, Brault J, Daudin B and Jalabert D 2003 *J. Appl. Phys.* **94** 2755–7
Berz F and Kuiken H K 1976 *Solid-State Electron.* **19** 437–45
Bylander E G 1978 *J. Appl. Phys.* **49** 1188–95
Chauveau J-M, Laügt M, Venneguès P, Teisseire M, Lo B, Deparis C, Morhain C and Vinter B 2008 *Semicond. Sci. Technol.* **23** 035005
Davidson S M 1977 *J. Microsc.* **110** 177–204
Donatini F, Luna de Bugallo A, Tchoulfian P, Chicot G, Sartel C, Sallet V and Pernot J 2016a *Nanoletters* **16** 2938–44
Donatini F, Arnold C and Barjon J 2016b private communication
Donolato C 1994 *Phys. Status Solidi* a **14** K131–32
Donolato C 1982 *Solid-State Electron.* **25** 1077–81
Drouin D, Couture A R, Joly D, Tastet X, Aimez V and Gauvin R 2007 *Scanning* **29** 92–101
Gustafsson A, Pistol M-E, Montelius L and Samuelson L 1998 *J. Appl. Phys.* **84** 1715–75
Hwang J-S, Donatini F, Pernot J, Thierry R, Ferret P and Dang L S 2011 *Nanotechnology* **22** 475704
Im J S, Moritz A, Steuber F, Härle V, Scholz F and Hangleiter A 1997 *Appl. Phys. Lett.* **70** 631–3
Kaschner A *et al* 2002 *Appl. Phys. Lett.* **80** 1909–11
Klingshirn C F, Meyer B K, Waag A, Hoffmann A and Geurts J 2010 *Zinc Oxide From Fundamental Properties Towards Novel Applications* (*Springer Series in Materials Science*) (Berlin: Springer)
Langer J M and Walukiewicz W 1995 *Mater. Sci. Forum* **196–201** 1389
Matsuo H, Kobayashi N, Kimura Y and Shimizu R 1996 *J. Electron Microsc.* **45** 453–57
Noltemeyer M, Bertram F, Hempel T, Bastek B, Polyakov A, Christen J, Brandt M, Lorenz M and Grundmann M 2012 *J. Mater. Res.* **27** 2225–31
Phillips M R 2006 *Mikrochim. Acta* **155** 51–8
Saritas M and McKell H D 1988 *J. Appl. Phys.* **63** 4561–7
Sekiguchi T, Liu Q, Tanaka T, Hu J, Zhu Y and Bando Y 2004 *Eur. Phys. J. Appl. Phys.* **27** 107–9
Yoo J, Yi G-C and Dang L S 2008 *Small* **4** 467–70
Yuan J, Berger S D and Brown L M 1989 *J. Phys.: Condens. Matter* **1** 3253–65
Zhao Q X, Yang L L, Willander M, Sernelius B E and Holtz P O 2008 *J. Appl. Phys.* **104** 073526
Zippel J, Lenzner J, Benndorf G, Lange M, Hochmuth H, Lorenz M and Grundmann M 2009 *J. Vac. Sci. Technol.* B **27** 1735–40